Influence of Inlet Positions on the Flow Behavior Inside a Photoreactor

M. Poliński and Z. Stęgowski

Abstract Efficiency of a photoreactor depends on the irradiation dose. Fluid residence time distribution (RTD) reflects hydrodynamic behavior of the flow. A computational model was built on a base and fitting a previous radiotracer experiment. Results of three simulations for three different configurations and height flow rate are presented and discussed below. This paper shows usefulness of CFD modeling as an imaging tool, which can be used to retrieve detailed, local information about the flow.

Keywords Photoreactor · Residence time distribution · Tracers · CFD

1 Introduction

Effluent disinfection is often done in photoreactors, which consist of a set of UV lamps that irradiate the wastewater. Productivity of such apparatus depends on disinfection kinetics. Radiation intensity decreases with distance from the lamps with respect to exponential behavior according to Beer's law. In a perfect photoreactor, radiation dose would be equal in every fluid element. For this reason, flow shall be characterized with high mixing rate in tangential direction to UV lamps. Favored trajectory and stagnant zones should be reduced as much as possible, because their result downgrades the efficiency and raises operational costs. A variety of photoreactors designs was previously studied. One of the recent solutions was proposed by Moreira [1], who proposed a device with four vertical lamps, an upward flow and configurable inlets. They used it to conduct the radiotracers experiment in order to obtain Residence Time Distributions (RTD).

M. Poliński (✉) · Z. Stęgowski
Faculty of Physics and Applied Computer Science, AGH University of Science and Technology, al. Mickiewicza 30, 30-059 Kraków, Poland
e-mail: michal.polinski@fis.agh.edu.pl

P. Kulczycki et al. (eds.), *Information Technology and Computational Physics*, Advances in Intelligent Systems and Computing 462,
DOI 10.1007/978-3-319-44260-0_13

Data gathered during their investigation was used as a starting point and validation reference for numerical modeling. Computational Fluid Dynamics (CFD) methods was deployed. Workflow of reconstructing RTD using virtual prototyping methods was described by Sugiharto et al. [2] Furman and Stęgowski, respectively, [3] have described RTD–CFD the junction in case of axial mixing in a pipe flow. The RTD curve contains comprehensive information about flow pattern, but values like local velocity and local effective dissipation rate are hidden because of its integral nature. The objective of this work is to retrieve and to show detailed information about local values of the flow inside the photoreactor, which cannot be directly quantified during radiotracer measurement. This paper describes the used workflow and present hydrodynamic behavior in a photoreactor with various inlets set up.

2 Experimental Part

This work has its origin in the measurements performed by Moreira [1] at the Center for the Development of Nuclear technology in Belo Horizonte in Brazil. As mentioned in the introduction they designed and built the photoreactor as a vertical tube 875 mm tall and with a diameter of 200 mm. PVC tubes were used, because of their common availability. Authors claim that this design should be very simple to build and does not require sophisticated tools and expensive materials. A set of four UV lamps was mounted inside—also vertically. Outflow was placed near the top. Inflows were situated close to the bottom and they had a possibility to choose from three varied configurations:

- Configuration 1: One central bottom inlet,
- Configuration 2: One lateral inlet,
- Configuration 3: Three lateral inlets equally spaced around the bottom of the reactor with flowrate divided into three equal parts.

During their experiments, different configurations were tested with flow rates starting from 0.112 dm^3/s to 0.881 dm^3/s.

For this paper, the upper flowrate level cases were chosen, because it emphasizes differences between the inlet configurations. To be precise, the following cases have been selected to in this paper:

- Simulation 1: 0.869 dm^3/s flow rate in one central bottom inlet setup (not done in experiment),
- Simulation 2: 0.869 dm^3/s flow rate in one lateral inlet set up,
- Simulation 3: 0.881 dm^3/s flow rate.

3 Residence Time Distribution

Residence time distribution (RTD) is a commonly used technique for describing flow patterns in a large class of applications, and particularly for investigating reactors. This term was first introduced by MacMullin and Weber in 1935 and the first application was proposed by Dankwerts [4] in 1953. Later it has been described in a multitude of scientific papers like Dudukovic [5] and Levenspiel [6].

Residence time distributions are usually obtained by injecting tracer at the examined flow inlet and then measuring its concentration at least at the outlet of the flow system. Normalized form of RTD could be treated as a probability distribution function for time space that describes the quantity of time a fluid element spends inside the flow system.

Injection of tracer shall not change the flow characteristics, so it shall be inert to the flow—have the same physical properties like density, viscosity, as the main fluid in the examined flow. Besides that, the substance chosen for the marker shall be clearly distinguishable from the current. There are multiple different approaches for the tracer choice. One of them is the use of a small amount of radioactive isotopes like proposed in Hector Constant-Machado et al. [7] Because emitting γ-radiation radiotracers are easy distinguishable and it is not needed to use high concentrations, they are also neutral for the flow. Emission of γ-radiation is proportional to the concentration of tracer in the flow. There are also other non-radioactive techniques for obtaining RTD, like the method that uses phosphorescent marker particles, which could be detected via light sensitive photomultiplier. An example of such measurements is shown in Harris et al. [8].

With an assumption of a constant flow rate RTD or the impulse response E(t) is usually defined as ratio of the outflow concentration $C_{out}(t)$ to the total amount of dissolved tracer.

$$E(t) = \frac{C_{out}(t)}{\int_0^\infty C_{out}(t)dt} \tag{1}$$

This is the simplest case, when inflow concentration $C_{in}(t)$ could be assumed as a Dirac delta function. For other cases, when injection is non-instantaneous $C_{out}(t)$ function is described as a product of the convolution of inflow $C_{in}(t)$ impulse by the impulse response E(t).

$$C_{out}(t) = \int_0^t C_{in}(t)E(t-x)dx \tag{2}$$

RTD experiments are a crucial concept to characterize flow and mixing inside the reactor. It helps to distinguish if the flow is close to one of opposed ideal reactor: plug reactor or perfect mixing reactor. The basic approach of examination RTD is a method of moments. The first moments of the measured residence time distribution yield the mean residence time in flow system. The second moment help

estimate the dispersion of tracer in the flow. Higher moments are also in use. In most cases, residence time distribution characterizes with positive skewness. The presence of stagnant zones in flow results with higher third moment.

Ideal plug flow reactor is characterized with no mixing in an axial direction. The fluid elements do not change their order during the flow, so residence time is equal for each single droplet of fluid. There is no dispersion at all, so the variance of an ideal plug flow reactor is equal to zero. Therefore, the residence time distribution is a Dirac delta function shifted by mean residence time T.

$$E(t) = \delta(t - T) \tag{3}$$

Another boundary case is a perfect mixing reactor also called a continuous stirred-tank reactor. This model is based on the assumption that inlet flow is continuously mixed with bulk volume of a reactor. All the time the outflow has the same uniform structure as the reactor volume. The residence time distribution for the perfect mixing reactor is described by exponential decay that is:

$$E(t) = \frac{1}{T} e^{-\frac{t}{T}} \tag{4}$$

Any residence time distribution could be mathematically described as a superposition of ideal plug flow reactors and perfect mixing reactors. Many compartment models were proposed to explain flow behavior. The agreement of such modeling with experimentally obtained RTD grows with number of blocks, compartments used to build a model—starting from one plug flow reactor with junction of one perfect mixing cell like proposed in Moreira [1] paper up to twenty shown by Hocine et al. [9]. Another examples of this quasi analytical approach for flow modeling could be found in Hocine [10], Haris et al. [8, 11] and also in Blet et al. [12].

As it is shown in the Fig. 1 the RTD describes the flow in black box manner, so in case to deeply analyze the flow it must be combined with another method like previously described method of moments or compartment models. Anyway it could be also used as a rich comparison data for direct simulation methods, because RTD data store information about whole flow in an integrate manner. For that reason, we use experimental residence time distributions as a reference point for computational fluid dynamics calculations to find what details have the highest influence for the stream.

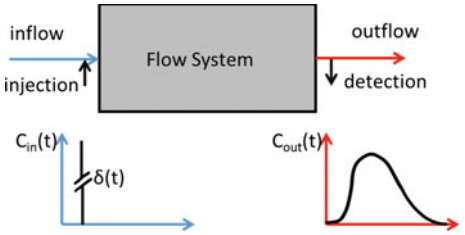

Fig. 1 Residence time distribution

4 Numerical Methods and Simulation Setup

Computational fluid dynamics (CFD) methods were used to model the flow in the photoreactor and then to simulate residence time distribution for each of chosen case. The commercial Fluent package [13] was used to drive the calculations. This section shortly presents governing equations and two-step workflow, which was used. First, the flow was calculated using a finite volume method. Therefore, particle tracking on previously calculated stationary flow was used to retrieve RTD.

4.1 Navier-Stokes Equations

The majority of fluid dynamics problems are solved using Navier–Stokes equations (N–S). This description of motion of viscous fluid substances is named after Claude–Louis Navier and George Gabriel Stokes and it was introduced in 1822. Until today, this set of equation has no analytical solution and smooth solutions to the Navier–Stokes equations are listed as one of the Millennium Prize Problems in mathematics, which are proposed by the Clay Mathematics Institute as the seven most important open problems in mathematics, with a reward of million US dollars for solving. They express the conservation of momentum principle. N–S equations are formed by applying Newton's second law of fluid motion with assumption that the stress in the fluid is the sum of the effects of viscosity and the effects associated with the pressure. Using Einstein's summation convention as follows:

$$\frac{\partial u_i}{\partial t} + u_j \frac{\partial u_i}{\partial x_j} = -\frac{1}{\rho}\frac{\partial p}{\partial x_i} + \rho\vec{g} + \overrightarrow{F_c} + \upsilon\frac{\partial^2 u_i}{\partial x_j \partial x_j} \tag{5}$$

where u_i denotes the velocity in Cartesian coordinates, t stands for time, p is pressure, density is denoted by ρ, kinematic viscosity is represented with υ. Gravitational acceleration is marked by $\vec{g}$ and $\overrightarrow{F_c}$ stands for Coriolis force.

Applying Eq. (5) together with conservation of mass, with assumption of incompressibility, i.e.,

$$\frac{\partial(u_i)}{\partial x_i} = 0 \tag{6}$$

results with complete psychical description for fluid in motion in Cartesian coordinates.

As it was mentioned above, there is as yet no smooth, general solution for the Navier–Stokes equation, but there are many specific solutions for particular problems, which are usually solved using dimensional analysis. Order of magnitude of each separate part of equations is calculated. Parts smaller than orders are neglected. For example, in laboratory scale, which shall be taken account in this paper the

gravitational acceleration $\vec{g}$ and Coriolis force $\overrightarrow{F_c}$ are negligible in comparison with viscous and pressure term. These assumptions yield

$$\frac{\partial u_i}{\partial t} + u_j \frac{\partial u_i}{\partial x_j} = -\frac{1}{\rho}\frac{\partial p}{\partial x_i} + \upsilon \frac{\partial^2 u_i}{\partial x_j \partial x_j} \tag{7}$$

Depending on the solving problem, different assumptions are also applied.

4.2 Reynolds Averaged Navier–Stokes Equation

The stationary Reynolds-Averaged Navier–Stokes (RANS) approach was used to drive the calculations of flow motion. It is the oldest and the best known way to model turbulent flow. The estimated Reynolds number for the investigated system is greater than 3,000. Therefore, mathematical model used to describe the flow needs to take into account its turbulent behavior. The method behind the equations is called Reynolds decomposition and it was firstly proposed by Osborne Reynolds [14] in 1895. Making an assumption that physical value averaged in time:

$$\underline{\varphi} = \frac{1}{\Delta t}\int_0^{\Delta t} \varphi_{(t)} dt \tag{8}$$

could be described as a sum of time average and fluctuations around it:

$$\varphi = \underline{\varphi} + \varphi' \tag{9}$$

Fluctuating part averaged in time in the same manner as shown above is equal to zero. These assumptions put inside the momentum conservation law yields

$$\frac{\partial u_i}{\partial t} + u_j \frac{\partial u_i}{\partial x_j} = -\frac{1}{\rho}\frac{\partial \underline{p}}{\partial x_i} + \upsilon \frac{\partial \underline{u_i}}{\partial x_j \partial x_j} - \rho \frac{1}{\partial x_j}\underline{u_j' u_i'} \tag{10}$$

The left-hand side remains in the same form. Also the pressure derivative source term is not changing during Reynolds averaging. Fluctuations remain only in diffusion term. The component containing fluctuations is called the Reynolds stress tensor:

$$\tau_{ij}' = \underline{u_i' u_j'} \tag{11}$$

The term described by the equation above contains six unknown correlations, which is too many to solve the described system of equations and leads to closure problem. As a result another postulations need to be added. Due to this issue,

turbulence modeling has to be implemented to change the above equation system to the form of a closed set.

4.3 The Parameters Characteristic for Turbulence

Root mean squared average, which is also known as quadratic mean, could be calculated using the following definition:

$$\varphi'_{rms} = \sqrt{\frac{1}{\Delta t}\int_0^{\Delta t} (\varphi'_{(t)})^2 dt} \tag{12}$$

Applying the above formula to the term responsible for the turbulence kinetic energy per unit mass could be extracted, so the turbulence kinetic energy takes the form:

$$k = \frac{1}{2}\underline{u'_i u'_i} \tag{13}$$

Therefore, the amount of energy dissipated per unit mass, per unit time follows the rule:

$$\varepsilon = \frac{\upsilon}{2}\left(\frac{\partial u_i}{\partial x_j} + \frac{\partial u_j}{\partial x_i}\right) \tag{14}$$

4.4 Eddy Viscosity-Based Turbulence Models

Eddy viscosity-based turbulence models assumes the undefined Reynolds stress tensor using two hypotheses. The first one is the Boussinesq hypothesis, which involves the proportionality of Reynolds stress to the mean velocity gradients with proportional factor of turbulent viscosity υ_t. In our words, the Reynolds stress term behaves in the same way as viscosity stress.

$$\underline{u'_i u'_j} = -\upsilon_t\left(\frac{\partial u_i}{\partial x_j} + \frac{\partial u_j}{\partial x_i}\right) - \frac{2}{3}\delta_{ij}k \tag{15}$$

where δ_{ij} is a Kroneker delta function and υ_t denotes the turbulent viscosity. It is a scalar value, which means that it is assumed to be isotopic. The minus sign before the right-hand side means that turbulence tends to stop the flow via turbulence viscosity, which is taking energy from main stream and transport it to another direction.

The first turbulence model was proposed by Ludwig Prandtl in 1925 [15]. The mixing length model supposes eddy viscosity to be proportional to a velocity scale with a proportionality constant described by turbulent length scale L, that is,

$$\upsilon_t \propto LU \tag{16}$$

4.5 K-Epsilon RNG Equations

Applying dimensional analysis to the Eq. 11 velocity scale U could be described as a square root of turbulence kinetic energy $\sqrt{k}$ and then turbulent length scale L could be qualifying as by largest existing scale of turbulence in examined problem. There are many different approaches to choice the length scale L and there are depending on specified turbulent quantity. The k-ε RNG was employed in this paper. It relates the turbulent length scale to a kinetic energy dissipation rate ε, so the turbulent viscosity is expressed as

$$\upsilon_t = C_\mu \frac{k^2}{\varepsilon} \tag{17}$$

Proportionality constant C_μ is an empirical value. It is usually taken as 0.09.

The transport equations for the turbulence kinetic energy k and its dissipation rate ε are shown in the Eqs. 14 and 15.

$$\rho u_i \frac{\partial k}{\partial x_i} = \mu_t \left(\frac{1}{2} \left(\frac{\partial u_j}{\partial x_i} + \frac{\partial u_i}{\partial x_j} \right) \right)^2 + \frac{\partial}{\partial x_i} \left(\alpha_k \mu_{eff} \frac{\partial k}{\partial x_i} \right) - \rho\varepsilon \tag{18}$$

$$\begin{aligned} \rho U_i \frac{\partial \varepsilon}{\partial x_i} = {} & C_1 \left(\frac{\varepsilon}{k} \right) \mu_t \left(\frac{1}{2} \left(\frac{\partial u_j}{\partial x_i} + \frac{\partial u_i}{\partial x_j} \right) \right)^2 \\ & + \frac{\partial}{\partial x_i} \left(\alpha_\varepsilon \mu_{eff} \frac{\partial \varepsilon}{\partial x_i} \right) - C_2 \rho \left(\frac{\varepsilon^2}{k} \right) - R \end{aligned} \tag{19}$$

R is an additional scalar related to mean strain and turbulence quantities. This model was chosen because of an opportunity to account for the effects of smaller scales of motion. It was designed to improve accuracy in simulation of rotating flows, therefore mixing results also. A detailed description of k-epsilon RNG model and constant values can be found in Yakhot et al. [16] and Tennekes and Lumley [17].

4.6 Finite Volume Method and Boundary Conditions

Solving the equations for fluid main velocity (10) and its turbulence parameters (18), (19) requires the use of numerical methods. These equations were discretized on the numerical mesh using the finite volume method (FEM). This numerical approach represents analytic form of partial differential equations in shape of set of algebraic equations. Values are solved on a discrete computational mesh made up from set of small finite volumes. Using Gauss-Ostrogradsky's theorem divergence terms are converted into surface integral. The flow is discretized to the form of fluxes at the surfaces between adjacent finite volumes.

The zero step, when applying FVM, is to create system geometry and mesh, which follows corresponding dimensions of experimental setup. Tetrahedral mesh was used for creating the computational grid. There were approximately 3,000,000 cells used. It is shown in Fig. 2.

The following boundary conditions were used:

- No-slip wall boundary condition was set on the photoreactor sides—zero velocity and standard wall functions for flow calculations and reflection for discrete phase motion were assumed.

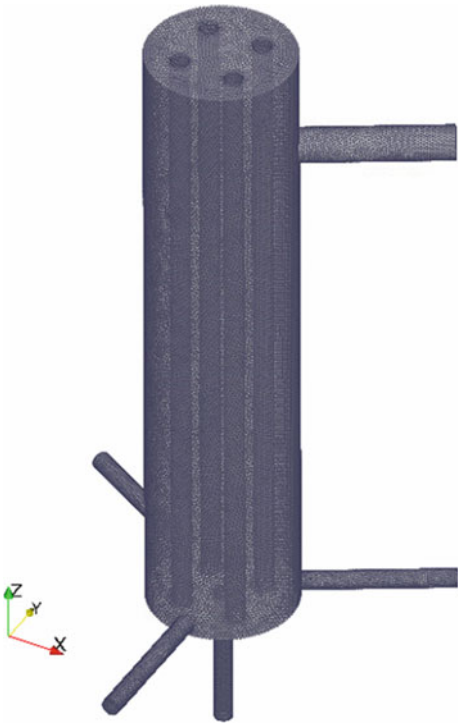

Fig. 2 Computational mesh

- Velocity inlets for inlet surfaces with constant velocity profile. In order to obtain physically correct axial velocity profile at the entrance to photoreactor inflow tubes was additionally extended.
- Outflow boundary condition was set for the outlet.

4.7 Particle Tracking

Simulating Residence time distribution requires additional calculations to the previously calculated stationary flow. Using prior simulated velocity field, a particle tracking method was deployed to retrieve RTD. Similar approach as described by Zhang and Chen [18], Cantu-Perez et al. [19, 20] was used. Numerous trajectories were simulated using the Lagrangian particle tracking method in case to collect statistics and determine probability distribution function.

For each simulation, more than 10,000 individual particle tracks were calculated. Particles were described with the same physical values as fluid volume. The droplet size d was set at 10^{-6} m, which is a value far below the size of the involved computational grid. Particle motion is driven by the Stokes drag law and it is described by the equation:

$$\frac{du_{i,p}}{dx} = \left(\frac{\upsilon 18}{d^2 C_c}\right)\left(\underline{u_i} - u_{i,p}\right) \tag{20}$$

Discrete random walk (DRM) model was used to simulate stochastic velocity fluctuations in the flow. The fluctuating velocity component follows Gaussian probability distribution and is proportional to the turbulent kinetic energy k calculated in the previous step that is:

$$u_i^{'} = \zeta\sqrt{\frac{2}{3}k} \tag{21}$$

5 Results and Discussion

This section presents the results of the conducted simulations. On the experimental field, it was not possible to look inside the flow. One of the reasons was that photoreactor sides have to be painted black, because of safety reasons resulting from the use of UV and γ radiation. Various measurement techniques like particle image velocimetry [21], different kinds of anemometry are costly or flow disturbing. Applying CFD techniques flow could be analyzed without restrictions in any place inside the system, but in need of a fit to experimental data. RTD measurements are taken at the inlet and outlet of the system and it covers information about

the whole flow, but any particular local information must be recalculated and resituated from it. Many simulation loops were done to obtain the best fit with experimental data.

The most intuitive way to describe the flow is visualization of velocity field. It is presented in two ways. Mean velocity trajectories are shown in Fig. 3.

Detailed local velocity directions are presented in Fig. 4 as vectors applied to horizontal cross-sections.

It can be observed that in the central inlet configuration a big part of volume is a stagnant zone, which is omitted by a mean flow. Introduction of lateral inlet configuration produces a swirling flow with significantly decreased stagnant zone. One lateral inlet is characterized by large spin. At the bottom part, it results with height rates velocities close to the sides. It produces local pressure drop in the center, which is the origin of the backflow. Dividing input flow into free lateral inlets, a swirling part of the flow was decreased as well. Opposite inlet position results with the most balanced axial velocity profile of all simulated cases.

Another interesting value that should be shown is effective viscosity, which is proportional to diffusion coefficient. It is described by equation X and it contains both physical values describing the turbulence: turbulent kinetic energy k and dissipation rate ε. The photoreactor should be characterized by a high mixing rate in tangential direction to the UV lamps. Effective viscosity rate inside it is presented on vertical cross-sections shown in Fig. 5.

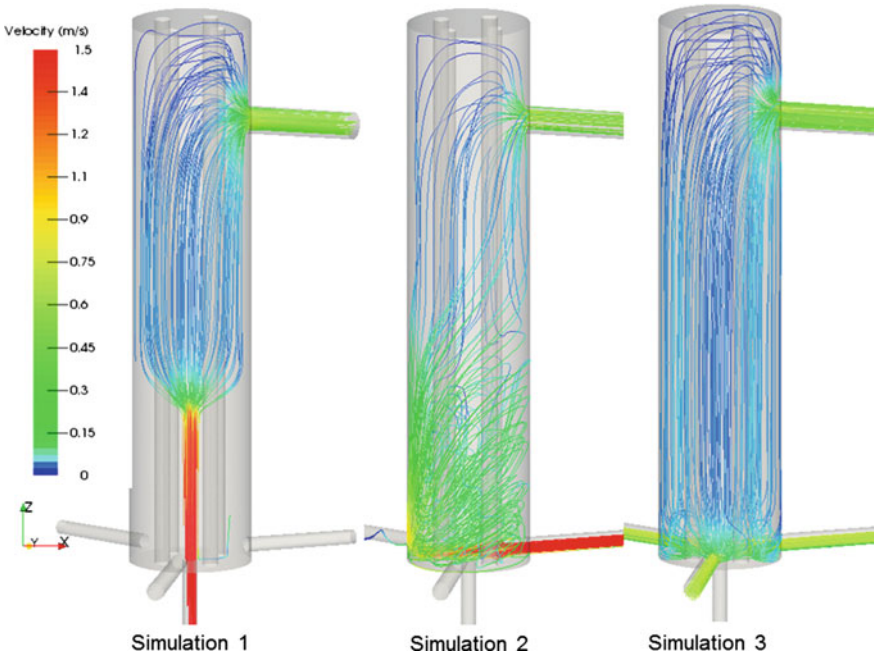

Fig. 3 Mean velocity streamlines

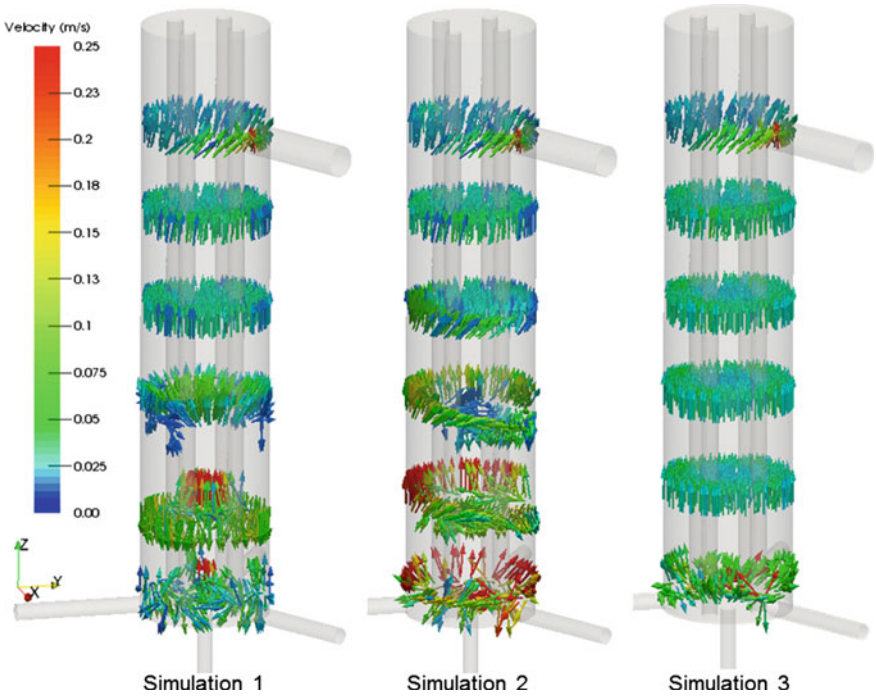

Fig. 4 Velocity Vectors

Water viscosity in a standard state is approximately equal to 0.001 kg/ms so the greater part of effective viscosity is the turbulence viscosity. As is describes the rate of subgrid motion, it is related to dispersion in small scales. There are significant differences between tested configurations, but in all cases the highest effective viscosity is in the center. Spin inside photoreactor is the highest in the simulation 2 case, which is also characterized by the lowest small scales motion. The highest viscosity rate is in the simulation 3 case, which is desired. It is likely to have high exchange rate close to the UV lamps in case of getting the dose per particle as equal as possible. Turbulent viscosity rate affects the specific particle path. Figure 6 presents 5 specific particle tracks.

In the illustration for simulation 1 it could be seen that in the bottom side parts, where the velocities are negligible in comparison to the main jet in the center, there is still a little movement. It might be called a dead zone, but it is not one, because there is still fluid exchange between the bottom and upper part of the system. Particles that are crossing through this stagnant zone are characterized by very long residence time in the system. It is desired to avoid such situations, because it has a tendency of an unnecessary overdose. As it was described earlier, simulation 2 has the lowest turbulence part and it produces the sharpest particle trajectories. Anyway, the backflow in the center results with trajectories with long overall residence time. Trajectories in simulation 3 case are fuzzy.

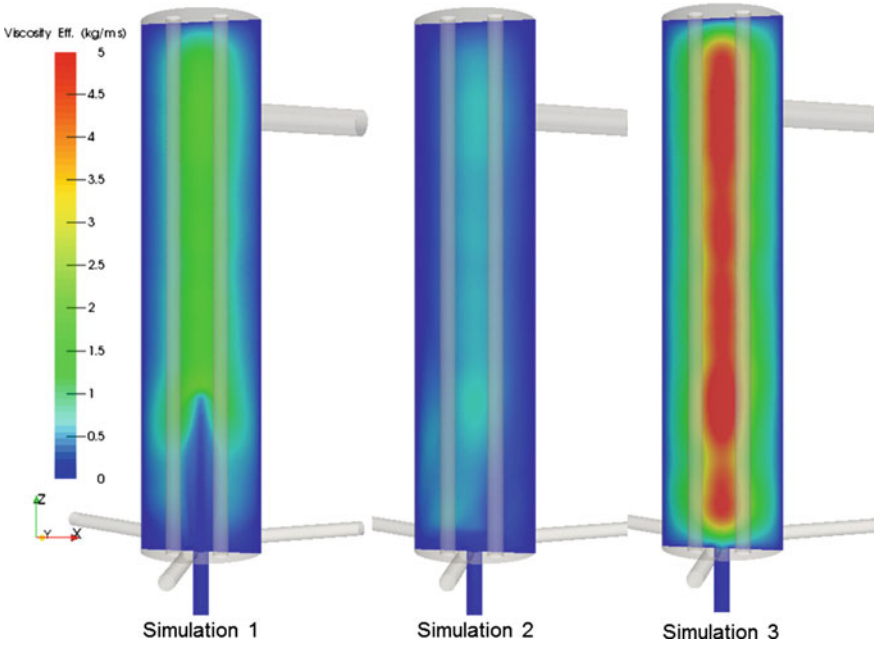

Fig. 5 Effective velocity field

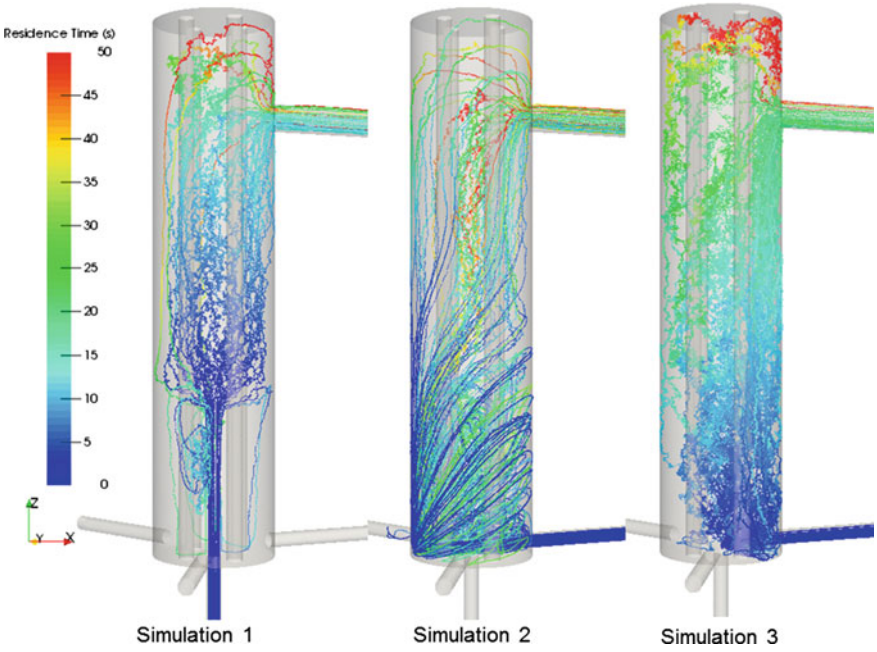

Fig. 6 Specific particle trajectories

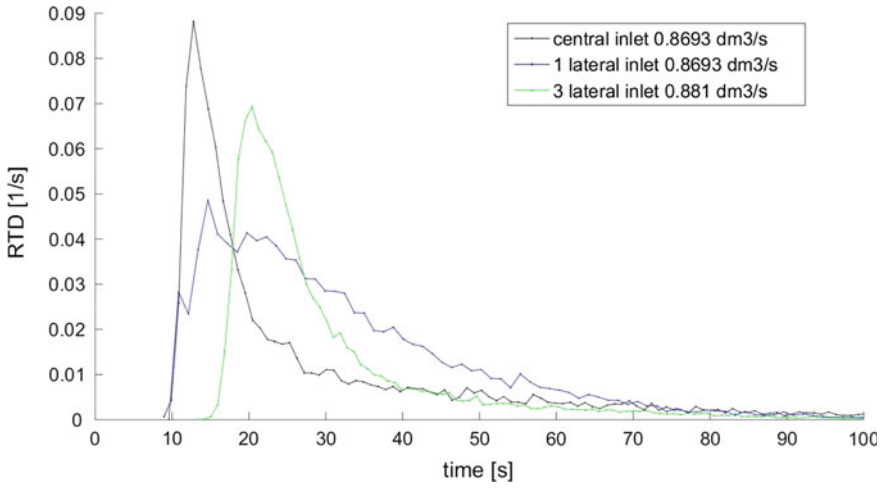

Fig. 7 Residence time distribution

The most equal axial velocity profile in that case results with that particle residence time tends to be proportional to the distance from the inlet. All flow characteristics described below lead to different shape of RTD. It was calculated as an overall particle residence time in the system for many simulated particles. For each curve shown in Fig. 6, more than 10,000 individual particle tracks were calculated.

As could be expected there are major differences between obtained RTDs, which is presented on Fig. 7.

6 Conclusion

This paper shows the use of computational fluid dynamics methods in case to illustrate and comment on flow behavior in the photoreactor previously investigated by a radiotracer experiment. Computer simulation could be used to retrieve detailed, local information about the flow. It is also convenient for retrieving residence time distributions. The height flow rate was chosen to emphasize the differences between three different inlet configuration. Major contrast between three investigated setups was shown. Simulation 2 is the worst case. It characterizes with big spin, which results with presence of undesired backflow. It has widely spread RDT, so radiation dose would differ much over the fluid elements. Simulation 1 case has the narrowest RDT over all simulated cases, which is expected regarding to fact that equal radiation dose distribution is one of the goals in photoreactors design. From the other hand, it produces big stagnant zone at the inlet side, which results with wasting the active volume of an apparatus. Approximately one-third of volume is out of the main stream and stays inside a photoreactor for a much longer time. That

fluid part might collect too high a radiation dose and its reduce dose collected by main stream. Simulation 3 has RTD somewhere in between the other two, so it might not be found as the best solution, when looking only at the RTD curve. Using CFD simulation, it could be seen that it also has the most balanced axial velocity profile and characterizes with the highest small-scale mixing rate, so it tends to be a most efficient set up in all test cases. In all three simulations there is still room for improvement near the outlet, because the upper part of volume above the outlet results with prolongation of residence time. This work describes hydrodynamic behavior of the flow inside the photoreactor, but its efficiency is also associated with disinfection kinetics. It shall be taken account in the succeeding investigations as well as the outflow design.

Acknowledgements The authors acknowledge the support of originators [1] for providing experimental data needed to lead simulations made for this research. This research was supported in part by PL-Grid Infrastructure. M.P. acknowledges his benefit from Ph.D. scholarships founded by Marian Smoluchowski Cracow Scientific Consortium—KNOW.

References

1. Moreira, R.M., Pinto, A.M.F., Mesnier, R., Leclerc, J-P.: Influence of inlet positions on the flow behaviour inside a photoreactor using radiotracers and colored tracer investigation. Appl. Radiat. Isot. **65**, 419–427 (2004)
2. Sugiharto, S., Stegowski, Z., Furman, L., Su'Ud, Z., Kurniadi, R., Waris, A., Abidin, Z.: Dispersion determination in a turbulent pipeflow using radiotracer data and CFD analysis. Comput. Fluids **79**, 77–81 (2013)
3. Furman, L., Stęgowski, Z.: CFD models of jet mixing and their validation by tracer experiments. Chem. Eng. Process. **50**(3), 300–304 (2011). ISSN 0255-2701
4. Danckwerts, P.V.: Continuous flow systems, distribution of residence times. Chem. Eng. Sci. **2**(1), 1–13 (1953)
5. Dudukovic, M.P.: Tracer methods in chemical reactors. Techniques and applications. Chem. React. Des. Technol., NATO ASI Series (1986)
6. Levenspiel, O.: Chemical Reaction Engineering, 3rd edn. Wiley, New York (1999)
7. Constant-Machado, H., Lecrerc, J.P., Avilan, E., Landaeta, G., Anorga, N., Capote, O.: Flow modeling of a battery of industrial crude oil/gas separators using ^{113m}Im tracer experiments. Chem. Eng. Process. **44** (2005)
8. Haris, A.T., Davidson, J.F., Thorpe, R.B.: A novel method for measuring the residence time distribution in short time scale particulate systems. Chem. Eng. J. **89** (2002)
9. Hocine, S.: Identification de modeles de procedes par programmation mixte deterministe. Ph. D. thesis, INP Toulouse (2006)
10. Hocine, S., Pibouleau, L., Azzaro-Pantel, C., Domenech, S.: Modelling systems defined by RTD curves. Comput. Chem. Eng. **32** (2008)
11. Haris, A.T., Davidson, J.F., Thorpe, R.B.: Particle residence time distributions in circulating fluidised beds. Chem. Eng. Sci. **58** (2003)
12. Blet, V., Berne, Ph., Chaussy, C., Perrin, S., Schweich, D.: Characterization of a packed column using radioactive tracers. Chem. Eng. Sci. (1999)
13. FLUENT Inc., FLUENT 6 User's Manual, 2006
14. Osborne, R.: On the dynamical theory of incompressible viscous fluids and the determination of the criterion. Philos. Trans. R. Soc. London A **186**, 123–164 (1895)

15. Prandtl, L.: Z. angew. Meth. Mech **5**(1), 136–139 (1925)
16. Yakhot, V., Orszag, S.A., Thangam, S., Gatski, T.B., Speziale, C.G.: Development of turbulence models for shear flows by a double expansion technique. Phys. Fluids A **4**(7), 1510–1520 (1992)
17. Tennekes, H., Lumley, J.L.: A First Course in Turbulence.
18. Zhang, Z., Chen, Q.: Experimental measurements and numerical simulation of particle transport and distribution in ventilated rooms. Atmos. Environ. **40**, 419–427 (2006)
19. Cantu-Perez, A., Barrass, S., Gavriilidis, A.: Residence time distributions in microchannels: comparison between channels with herringbone structures and rectangular channel. Chem. Eng. J. **160** (2010)
20. Cantu-Perez, A., Barrass, S., Gavriilidis, A.: Hydrodynamics and reaction studies in a layered herringbone channel. Chem. Eng. J. **167** (2011)
21. Pruvost, J., Legrand, J., Legentilhomme, P., Doubliez, L.: Particle image velocimetry investigation of the flow-field of a 3D turbulent annular swirling decaying flow induced by means of a tangential inlet. Exp. Fluids **29** (2000)